Earth and Planetary Science Letters 482 (2018) 201–212

Contents lists available at ScienceDirect

Earth and Planetary Science Letters

www.elsevier.com/locate/epsl

Rapid geomagnetic field intensity variations in the Near East during the 6th millennium BC: New archeointensity data from Halafian site Yarim Tepe II (Northern Iraq)

Stanislava Yutsis-Akimova [a,b,*], Yves Gallet [a], Shahmardan Amirov [c]

[a] Institut de Physique du Globe de Paris, Sorbonne Paris Cité, Université Paris Diderot, UMR 7154 CNRS, F-75005 Paris, France
[b] Institute of Physics of the Earth, Russian Academy of Sciences, Moscow, Russia
[c] Archeological Institute, Russian Academy of Sciences, Moscow, Russia

ARTICLE INFO

Article history:
Received 21 June 2017
Received in revised form 13 October 2017
Accepted 4 November 2017
Available online xxxx
Editor: M. Frank

Keywords:
archeointensity
secular variation
pottery
Near East
Late Neolithic
Halaf

ABSTRACT

We present new archeointensity results from a series of groups of pottery fragments that were collected from the multi-layered archeological site Yarim Tepe II in Northern Iraq (Northern Mesopotamia) dated to the 6th millennium BC. This site comprises a 7-m-thick sequence of archeological deposits encompassing the Middle Halaf, Late Halaf and the Halaf-Ubaid Transitional (HUT), between ∼5750 and ∼5000 BC according to the chronology currently considered for the Halafian archeological period. Three new radiocarbon dates obtained from bone fragments confirm that Yarim Tepe II was likely not occupied before the Middle Halaf, as was independently established from archeological constraints. Archeointensity determinations were carried out using the protocol developed for the Triaxe magnetometer. This procedure takes into account thermoremanent magnetization anisotropy and cooling rate effects. 114 fragments fulfilled our set of archeointensity selection criteria, with intensity data obtained from at least two but most often three specimens per fragment. Mean archeointensity values were estimated for 23 groups of fragments well distributed across the entire stratigraphic sequence from the averaging of the data obtained from a minimum of three fragments per group. These values were dated using a bootstrap procedure relying on the stratigraphic position of the different groups of fragments and on the different age constraints available inside the Yarim Tepe II sequence. The new data show a significant decrease in geomagnetic field intensity by ∼12 μT between the Middle Halaf and the Late Halaf–HUT time interval. This decrease was accompanied by a short intensity peak, which may have lasted only a few decades, around the Middle Halaf–Late Halaf boundary, at ∼5500 BC. This evolution is quite similar to that observed from Syrian and Bulgarian archeointensity data, even though the precise duration of the intensity peak is presently questionable. The Bulgarian data set further suggests that the intensity secular variation in the Near East and in Eastern Europe during the 6th millennium BC was in fact principally punctuated by two successive short-lasting intensity peaks, the first around 5800 BC and the second around 5500 BC. The scarcity of the intensity data available worldwide, however, prevents us constraining the geomagnetic dipole or non-dipole origin of these features. The variation rates associated with the rapid intensity fluctuations observed in Yarim Tepe II are of ∼0.15–0.25 μT/yr. This range of values appears similar to that of rapid intensity variations that sporadically occurred in more recent times, such as in Western Europe around 700 BC and 1000 AD. In contrast, it is lower than the variation rates that were proposed for geomagnetic spikes. Our results also have interesting implications on Halafian archeology; in particular, they suggest that the Late Halaf–HUT boundary was older by ∼ one century than previously considered.

1. Introduction

Episodes of rapid, perhaps even extreme geomagnetic field variations are gaining interest throughout the archeomagnetism and geomagnetism communities. This interest has come to the fore with the discovery of archeomagnetic jerks and of geomagnetic spikes, as originally proposed by Gallet et al. (2003) and Ben-Yosef et al. (2009), respectively. These two geomagnetic features involve relative intensity maxima, but between them, the nature of the peaks strongly differs in both amplitude and duration.

* Corresponding author.
E-mail address: akimova@ipgp.fr (S. Yutsis-Akimova).

https://doi.org/10.1016/j.epsl.2017.11.013
0012-821X/

According to Ben-Yosef et al. (2009) and Shaar et al. (2011), the geomagnetic spikes would last less than 30–50 yr and the associated intensity variation rates would reach up to several μT/yr, a value much higher than the maximum rate of intensity variations known for the recent geomagnetic field (∼0.10 μT/yr; e.g. Livermore et al., 2014). Owing to the fact that the uppermost part of the liquid outer core is probably stratified (e.g. Hirose et al., 2013), the spike events would not be compatible with our present understanding of core flow patterns at the core surface. In particular, the mean velocity of the core-surface flows would need to be increased during only a few decades by a factor of ∼5 to 8 with respect to that characterizing the recent field behavior (Livermore et al., 2014). Consequently, the geomagnetic spikes, if confirmed, would probably require the existence of yet poorly known core processes. Although less extreme and apparently compatible with the core-surface flow patterns currently envisaged (e.g. Dumberry and Finlay, 2007), the origin of archeomagnetic jerks detected so far in Western Europe remains also quite uncertain. Gallet et al. (2009) suggested that they could reflect episodes of maximum geomagnetic field hemispheric asymmetry, but this interpretation still requires confirmation.

It remains that both archeomagnetic jerks and geomagnetic spikes require further testing (e.g. Gallet et al., 2014; Shaar et al., 2016; Hervé et al., 2017). Fournier et al. (2015) recently showed that a confirmation of the geomagnetic spikes through their possible effects on radionuclide production is far from being straightforward. It would also be pointless to seek corroborative evidence of these geomagnetic features in the global archeomagnetic field models covering the past few millennia (e.g. Pavón-Carrasco et al., 2014; Nilsson et al., 2014), as their resolution is strongly penalized by the uneven temporal and geographical distributions of the available data used to build the models. Therefore, their reliability can only be established from the acquisition of new archeointensity results.

In archeomagnetism, if we except cases of pure chance (e.g. Ertepinar et al., 2012) or a result originating from a large collection of precisely-dated data obtained from different sites at a regional scale (e.g. Genevey et al., 2013, 2016; Gallet et al., 2014; Hervé et al., 2017), the observation of rapid or extreme geomagnetic events requires specific sampling conditions. In the case of the geomagnetic spikes dated to the beginning of the first millennium BC discovered in the Levant, Ben-Yosef et al. (2009) and Shaar et al. (2011) analyzed copper slags collected from a series of layers rapidly accumulated due to intense metallurgical activity. Similar conditions also prevailed in certain archeological sites comprising a succession of numerous superimposed archeological layers, each of them characterizing a short-lasting occupation level. Multi-layered settlements are relatively numerous in the Near East or in Eastern Europe (e.g. Bulgaria) and their significant potential for recovering a time-sequential record of the field variations was underlined for instance by Kostadinova-Avramova et al. (2014) (see also Gallet et al., 2014 or Shaar et al., 2016).

In addition to the spikes detected at the beginning of the first millennium BC, Gallet et al. (2006, 2014) proposed in the Near East three periods also characterized by short-lasting (∼100–200 yr) intensity peaks: around 2600 BC, ∼2300 BC and ∼1500 BC. For older periods, before the Early Bronze Age (i.e. beyond ∼3000 BC), the available archeointensity data set is much more limited, precluding good knowledge of the intensity variations. However, Gallet et al. (2015) conducted an archeointensity study on potsherds sampled in Tell Halula and Tell Masaikh (Syria) dated to between the 7th and 6th millennium BC, i.e. during the late Neolithic (or Pottery Neolithic) period. Beyond the fact that these data are among the oldest archeomagnetic results obtained worldwide, Gallet et al. (2015) emphasized the excellent success rate of the archeointensity experiments carried out on ceramic fragments produced during the Halaf period (∼5900–5300 BC; e.g. Bernbeck and Nieuwenhuyse, 2013), a cultural phase remarkable for the quality of its ceramic production, with various shapes and extremely elaborate and beautifully painted decorations. The clay paste used for this production was fine and well fired in predominantly oxidizing conditions, which makes it a perfect target for archeomagnetic investigations. This interest is even more important because both Kovacheva et al. (2014) and Gallet et al. (2015) found significant and rapid geomagnetic field intensity variations during the 6th millennium BC.

Many Halafian sites were identified in Northern Mesopotamia and some of them were excavated in the past 100 yr, for instance Tell Arpachiyah, Yarim Tepe II in Northern Iraq and Tell Halaf, Tell Sabi Abyad, Chagar Bazar and Tell Halula in Syria (for a synthesis see for instance Akkermans and Schwartz, 2003; Nieuwenhuyse et al., 2013). Among these sites, Yarim Tepe II appears as a typical multi-layered settlement comprising a 7-m-thick sequence of archeological deposits. It was thoroughly excavated by Soviet archeologists in the early 1970s (e.g. Munchaev and Merpert, 1981). Today, this site is inaccessible, but fortunately most archeological remains (several thousands of potsherds, lithics and various objects including a few bone fragments) were transported to Moscow at the time of the excavations, listed and stored in a repository at the Archeological Institute. Thanks to this, here we present new archeointensity data obtained from a time-sequential series of groups of potsherds encompassing the entire thickness of the Yarim Tepe II deposits. Note that this work follows a previous study performed on the same archeological site by Nachasova and Burakov (1995), but which provided no information neither on the sampling nor on the archeomagnetic analyses. Our results therefore supersede the previous ones.

2. Archeological background and archeomagnetic sampling

The archeological site of Yarim Tepe II ($\lambda = 36°20'21''$N, $\varphi = 42°20'58''$E) is situated in Northern Iraq, in the modern province of Nineveh about 50 km westward from the city of Mosul (Fig. 1a). Historically, this territory belongs to Northern (or Upper) Mesopotamia. Several cultural phases were distinguished in this region during the Pottery Neolithic period, mainly from their ceramic productions: Proto-Hassuna and Archaic Hassuna, or pre-Halaf for a more general definition, during the 7th millennium BC, Hassuna/Samarra or Proto-Halaf, Halaf and Halaf-Ubaid Transitional (HUT) during the 6th millennium BC (see for instance, Akkermans and Schwartz, 2003; Nieuwenhuyse et al., 2013 and references therein).

In the late 1960s, a team of Soviet archeologists headed by R. Munchaev and N. Merpert discovered an ensemble of six hills over an area of ∼0.5 km^2 along the Dzhubara–Dyaryasi intermittent watercourse in the Tigris–Euphrates valley (Fig. 1b). Three mounds referred to as Yarim Tepe I/II/III revealed respectively the remains of three successive cultures, Hassuna, Halaf and HUT/Ubaid (Munchaev and Merpert, 1981). Intensive excavations were conducted until 1976 on the two most promising Yarim Tepe I and II sites. Here, we only focus on Yarim Tepe II. The hill is 100–120 m long, 50–60 m wide and 7 m high. This elongated shape is due to partial erosion by water flow (note that Yarim Tepe means “half of the hill” in Turkish). The excavations were undertaken in the central part of the hill on a surface of ∼600 m^2 (Fig. 1c). Even though the uppermost layers were disturbed by graves and pits emplaced in more recent times, they revealed ceramics similar to that discovered in Yarim Tepe III and dated to the HUT period. The virgin soil was reached immediately below the Halafian levels.

A detailed description of the excavations can be found in Munchaev and Merpert (1981) and Merpert and Munchaev (1993). Altogether, the deposits yield a 7.0-m-thick sequence of superim-

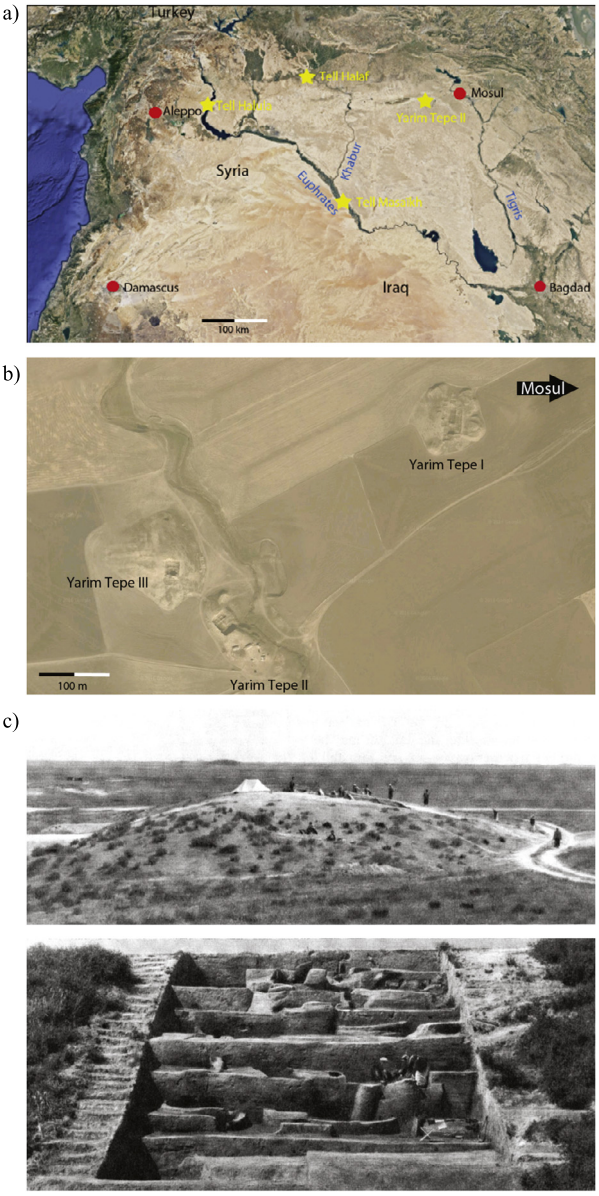

Fig. 1. General location map of Yarim Tepe II in the Near Eastern region (a). b) Satellite view of the three principal archeological sites discovered in Yarim Tepe (© Google Earth). c) View of the Soviet excavations conducted in Yarim Tepe II (© N.J. Merpert and R.M. Munchaev).

posed layers of occupation, divided into nine archeological levels based on the evolution in typo-morphology of ceramics. Each level contains from three to five superimposed stratigraphic layers, except level VII, which is very thin (about 30 cm). Our archeomagnetic sampling, relying on this subdivision, was performed from only three central digging squares in order to avoid as much as possible complexities that could be related to disruption in the lateral extension of the layers. The position of the potsherds was carefully checked according to the plans established by the archeologists and from the examination of the field notebooks containing all information on the excavations. We collected 30 groups of potsherds from successive stratigraphic layers across the entire Yarim Tepe II sequence, in most cases having a thickness of about 20 cm (Table 1; note that only one group of fragments was assembled for the very thin archeological level VII). Each group consists of at least three, up to 13 pottery fragments (see examples in Fig. 2). The latter were chosen following the fineness of the clay paste and their color, from light orange to light grey.

3. Methodology

All archeointensity results were obtained using the experimental protocol developed by Le Goff and Gallet (2004) for the three-axis vibrating sample magnetometer called Triaxe. This magnetometer allows continuous magnetization measurements of a small cylindrical specimen (volume <1 cm^3) directly at high temperatures (up to $\sim$700 °C). The Triaxe protocol is derived from the Thellier and Thellier (1959) method. The archeointensity analyses are performed between two temperatures referred to as T1 and T2, with T1 fixed to 150 °C and T2 generally chosen between 450 °C and 550 °C. Note that T2 is chosen to be not too high in order to minimize the possibility of alteration of the magnetic mineralogy during heating. After an initial heating of the specimen from room temperature to T1, the automated procedure involves a succession of five series of magnetization measurements made every $\sim$5 °C (M1 to M5; Le Goff and Gallet, 2004):

1. The specimen is first heated in zero field between T1 and T2, which allows the demagnetization of the NRM (series M1).

2–3. The specimen is then successively cooled down to T1 (series M2) and again heated up to T2 in zero field (series M3), in order to characterize the thermal variations of the NRM fraction still blocked at T2.

4. The specimen is cooled to T1 in a field (Hlab), the intensity of which is close to the expected ancient field intensity and the direction of which is such as the new laboratory TRM is acquired parallel to the NRM direction (series M4; see discussion in Le Goff and Gallet, 2004).

5. The specimen is heated to T2 in zero field in order to demagnetize the new laboratory TRM.

The experiments end with the rapid cooling of the specimen to room temperature. The entire cycle of measurements lasts slightly more than two hours.

From the magnetization data of series M1, M3 and M5 (acquired while the specimen is being heated), an estimate of the ancient field intensity (R′(Ti)) is obtained for each temperature Ti between T1 and T2 using the formula:

$$R'(Ti) = Hlab * \Delta'1(Ti)/\Delta'5((Ti)$$

Where

$$\Delta'1(Ti) = \big(M1(T1) - M1(Ti)\big) - \big(M3(T1) - M3(Ti)\big)$$
$$\Delta'5(Ti) = \big(M5(T1) - M5(Ti)\big) - \big(M3(T1) - M3(Ti)\big)$$

A mean intensity value is determined at the specimen level by averaging all the R′(Ti) data obtained between T1 and T2. In the case of a secondary magnetization component still existing above T1, this temperature can be changed into T1′ ($<$T2), so that the Triaxe intensity values are always determined from the characteristic/primary uni-vectorial magnetization of the archeological artifacts acquired during their manufacturing. A significant advantage of the Triaxe protocol is also that for each specimen, the mean R′(Ti) value takes into account both the anisotropy and cooling rate effects on TRM acquisition, as thoroughly discussed in Le Goff and Gallet (2004), Genevey et al. (2009) and Hartmann et al. (2010, 2011).

The reliability of the archeointensity values was evaluated through a set of selection criteria whose pertinence was clearly established in previous studies (e.g. Gallet and Le Goff, 2006; Gallet et al., 2006, 2015; Genevey et al., 2009, 2016; Hartmann et al., 2010, 2011). It is worth recalling that these criteria are applied at three levels: specimen, fragment and group of fragments. At the specimen level, the criteria concern the magnetic behavior observed during the Triaxe experiments, with the isolation of a well-defined characteristic thermoremanent magnetization and

Table 1
Archeological and archeomagnetic information on the groups of fragments studied in Yarim Tepe II. Columns 1 and 2: Name and archeological age of the groups of fragments. Columns 3 and 4: Stratigraphic position and modeled ages of the different groups of fragments. Columns 5 and 6: Mean intensity values and their standard deviations obtained before and after the use of a 3σ rejection test. Column 7: Number of fragments (N) and specimens (n) used to compute the mean intensity values provided in column 6.

Group of fragments	Archeological period	Depth (m)	Age (BC)	Intensity (μT)	Intensity 3σ (μT)	N frag. (n spec.)
YT01	HUT	0.20–0.40	5125 ± 56	33.6 ± 5.5	31.5 ± 2.1	5(15)
YT03	HUT	0.60–0.80	5162 ± 49	33.9 ± 4.6	31.9 ± 1.4	4(12)
YT04	HUT	1.00–1.20	5199 ± 44	31.4 ± 3.4	31.4 ± 3.4	3(8)
YT06	HUT	1.30–1.70	5237 ± 41	31.0 ± 3.4	29.7 ± 2.0	4(10)
YT07	HUT	1.70–1.85	5262 ± 38	33.3 ± 2.8	33.3 ± 2.8	3(9)
YT10	Late Halaf	2.15–2.40	5313 ± 36	30.8 ± 0.6	30.8 ± 0.6	3(6)
YT11	Late Halaf	2.20–2.40	5314 ± 36	31.9 ± 1.1	31.9 ± 1.1	3(9)
YT14	Late Halaf	2.80–3.20	5402 ± 30	31.1 ± 3.0	32.4 ± 1.6	3(8)
YT15	Late Halaf	3.20–3.40	5440 ± 25	32.4 ± 1.5	32.4 ± 1.5	3(9)
YT16	Late Halaf	3.20–3.60	5452 ± 29	32.6 ± 2.1	31.7 ± 1.0	3(9)
YT17	Late Halaf	3.40–3.70	5471 ± 27	30.9 ± 3.6	32.5 ± 1.5	3(9)
YT19	Late Halaf	3.60–3.90	5497 ± 29	31.4 ± 2.6	32.6 ± 1.1	3(8)
YT20	Late Halaf	3.70–4.00	5510 ± 30	32.5 ± 1.2	32.5 ± 1.2	6(17)
YT21	Late Halaf	4.40–4.60	5551 ± 20	34.5 ± 2.9	35.9 ± 1.3	3(8)
YT22	Late Halaf	4.60–4.70	5558 ± 21	43.2 ± 2.5	44.3 ± 1.4	3(8)
YT22A	Middle Halaf	4.80–5.20	5583 ± 21	32.4 ± 4.0	31.0 ± 2.3	5(12)
YT23	Middle Halaf	5.00–5.40	5611 ± 21	39.2 ± 4.5	39.2 ± 4.5	4(11)
YT24	Middle Halaf	5.50–5.70	5658 ± 20	43.8 ± 5.0	43.8 ± 5.0	5(15)
YT25	Middle Halaf	5.60–5.86	5672 ± 19	41.5 ± 3.6	43.1 ± 0.8	4(11)
YT26	Middle Halaf	5.90–6.20	5680 ± 18	43.4 ± 2.9	44.8 ± 0.9	3(9)
YT27	Middle Halaf	6.20–6.60	5701 ± 19	45.7 ± 2.1	45.7 ± 2.1	5(15)
YT28	Middle Halaf	6.50–6.75	5714 ± 18	46.4 ± 1.6	46.4 ± 1.6	5(15)
YT29	Middle Halaf	6.70–7.00	5737 ± 22	44.1 ± 2.3	43.1 ± 0.2	4(12)

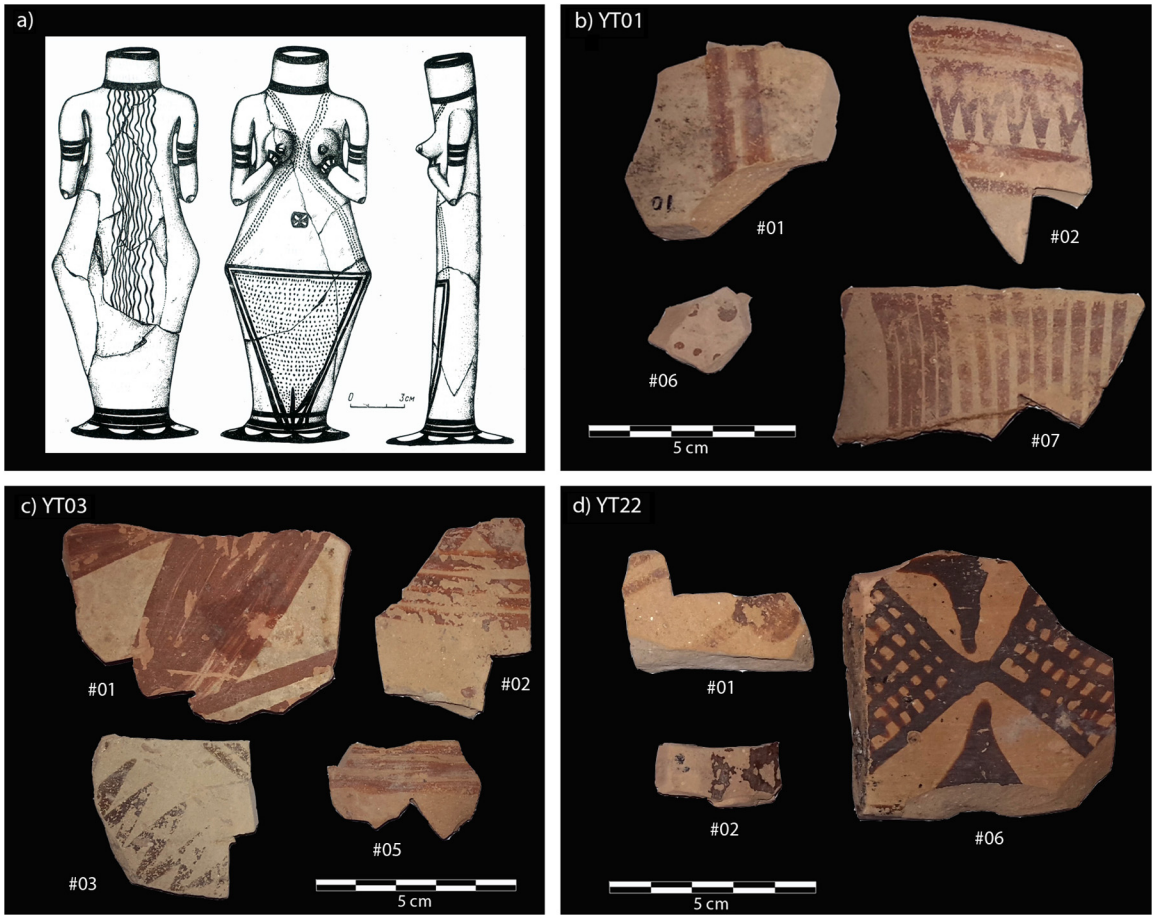

Fig. 2. Examples of ceramics discovered in Yarim Tepe II. a) Anthropomorphic clay vessel dated to the Middle Halaf (drawing from Merpert and Munchaev, 1993). b–d) Potsherds from groups YT01, YT03 an YT22 that provided archeointensity results satisfying our selection criteria. Note that one fragment from group YT01 (#05) is not shown as all material was used for the archeointensity analyses.

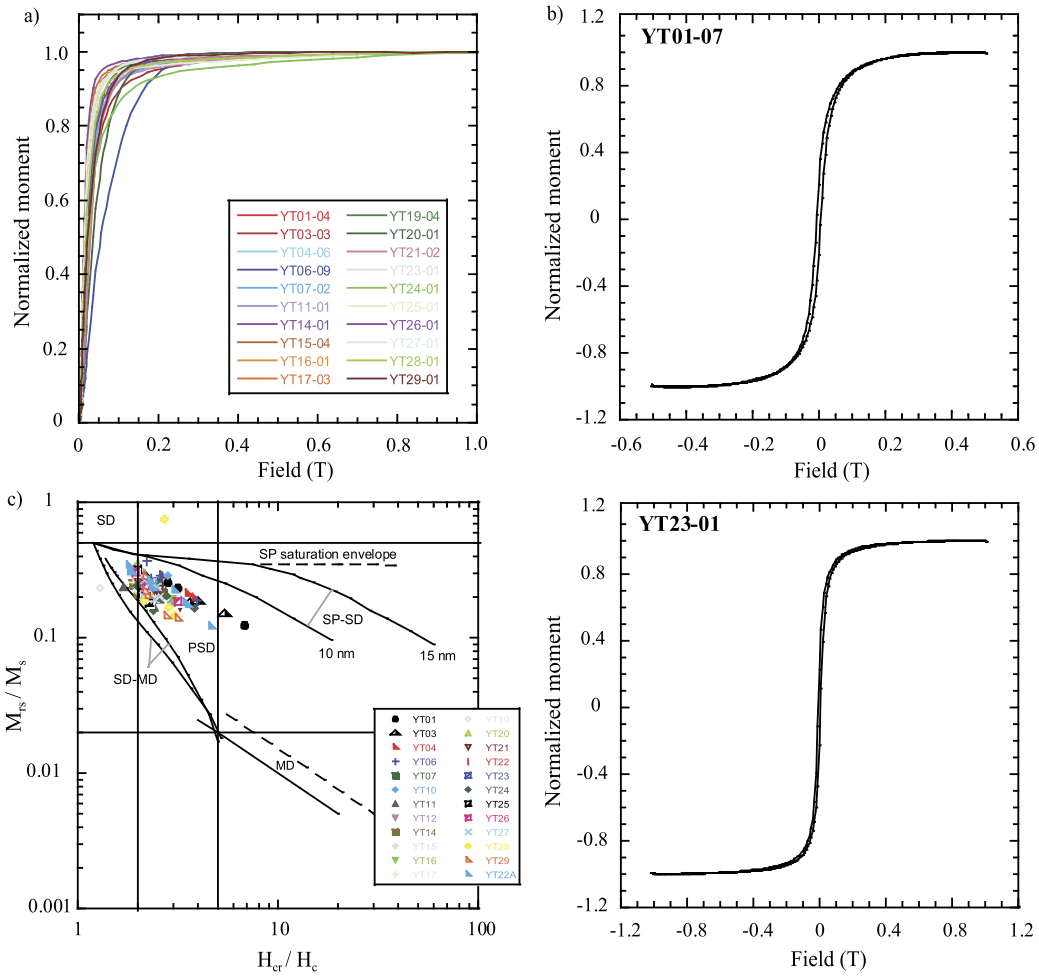

Fig. 3. Magnetic properties of pottery fragments from Yarim Tepe II. a) IRM curves acquired up to 1 T. b) Two examples of hysteresis loops. c) Distribution of the hysteresis ratios with zonation from Dunlop (2002). See Fig. S1 for additional IRM data obtained from other fragments.

with a nominal behavior for the R′(Ti) data as described in Le Goff and Gallet (2004). The R′(Ti) data vs temperature curves must show a linear and flat evolution, with a slope of less than 10%, and the magnetization fraction involved in archeointensity determination must be larger than 50% of the magnetization above T1/T1′. At the level of the fragment (potsherd) and at the level of each group of fragments, the criteria principally concern the consistency of the data. A fragment-mean intensity is considered only when at least two specimens give intensity values with a standard error ($n = 2$) or a standard deviation ($n = 3$) of less than 5% of the mean, whereas a group-mean intensity value is retained when at least three different fragments provide a mean intensity value with a standard deviation of less than 5 μT (Table S1).

In our study, we used an additional test to account for the fact that some groups of fragments may contain shards not representative (in time) of the archeological layers, where they were found. It is worth mentioning that such complexity, in the context of multi-layered settlements, is particularly critical. Indeed, for these sites, it may be extremely difficult if not impossible to ascertain the temporal homogeneity of the artifacts found in one particular stratigraphic layer. For a group of fragments, this may result in an intensity value significantly different from the other much less scattered values. In order to detect these fragments and eliminate the associated intensity values, we used a 3σ rejection test, assuming that a single shard at maximum for each group is possibly involved in such a perturbation. We conducted this test for each group containing at least four fragments successfully analyzed.

In addition to archeointensity measurements, rock magnetic experiments were carried out on all the fragments meeting our archeointensity selection criteria. These experiments, which aim to constrain the magnetic mineralogy of the fragments, include isothermal remanent magnetization (IRM) acquisition, hysteresis measurements and the acquisition of low-field susceptibility vs temperature curves.

4. Magnetic mineralogy

For all the retained fragments, the IRM measurements performed in fields up to 1 T show a magnetization saturation achieved between ∼0.3 T and ∼0.5 T (Fig. 3a), compatible with the presence of minerals from the (titano)magnetite family. Note that additional IRM data are shown in Fig. S1. The absence of high-coercivity minerals is further attested by the fact that the measured hysteresis loops are not constricted (Fig. 3b). In the Day diagram, the hysteresis ratios, with M_{rs}/M_s values ranging between ∼0.05 and ∼0.30 and H_{cr}/H_c values between ∼1.5 and ∼4.0, lie inside the area of pseudo-single domain (PSD) grains of magnetite (Fig. 3c; Dunlop, 2002).

The predominance of (titano)magnetite in our collection is also evidenced from the low-field susceptibility vs temperature curves carried out in most cases up to 600 °C. These curves show a clear inflexion point close to the Curie temperature of magnetite (Fig. 4 and Fig. S1). In some fragments, another inflexion point is observed in intermediate temperatures, around 350 °C, which may indicate the presence of magnetite with two main grain sizes or different

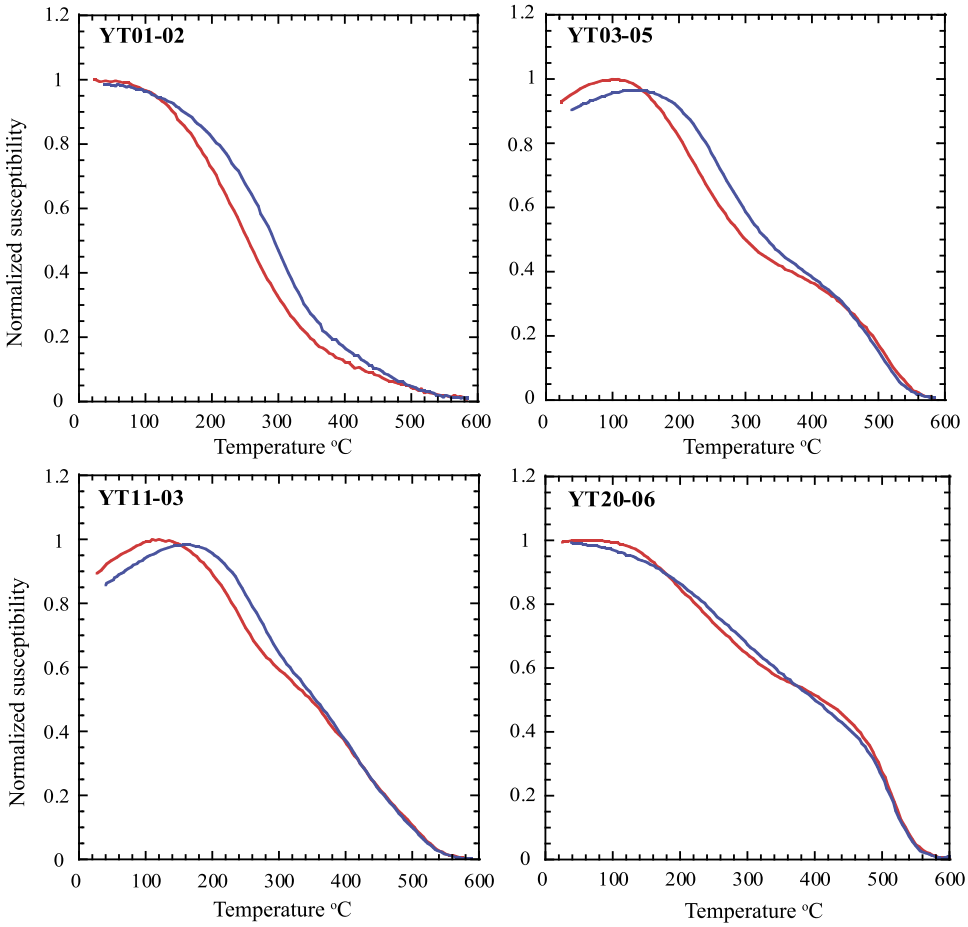

Fig. 4. Examples of low-field susceptibility vs temperature curves acquired up to 600 °C. In red the heating curves, in blue the cooling curves. See Fig. S1 for supplementary susceptibility data obtained from other fragments. (For interpretation of the references to color in this figure legend, the reader is referred to the web version of this article.)

titanium contents. It is worth pointing out that in all cases, the heating and cooling curves are reasonably well reversible, which further demonstrates the stability upon heating of the magnetic mineralogy of the fragments fulfilling our archeointensity selection criteria.

The magnetic mineralogy of the fragments from Yarim Yepe II hence appears very similar to that previously identified in the Halafian potsherds from Tell Halula and Tell Masaikh, and more generally to that observed for most Syrian ceramic fragments dated to the Bronze Age period (e.g. Genevey et al., 2003; Gallet et al., 2014, 2015).

5. New archeointensity results

We analyzed a total of 181 fragments (561 specimens). Among them, 114 fragments (321 specimens; Table S1) gave R′(Ti) data satisfying our archeointensity selection criteria. This corresponds to a success rate of ∼63%, quite similar to that achieved by Gallet et al. (2015) from Syrian Halaf potsherds. In a large proportion (94 fragments), the mean intensity values at the fragment level were determined from the data obtained from three different specimens (two specimens for the 20 remaining fragments).

Four examples of thermal demagnetization diagrams from retained fragments are shown in Fig. 5. A low unblocking temperature component, likely of viscous origin, is first isolated up to ∼150 °C. A secondary magnetization component is often observed up to ∼300–350 °C whose origin is probably linked to the fact that the associated pots were used in a culinary context. The characteristic or primary magnetization component is thus generally isolated over relatively high temperatures, often from ∼250 °C–350 °C up to ∼510 °C.

The rejection of fragments arose from three main causes: 1) a magnetization too weak to be measured with the Triaxe magnetometer (∼30% of rejected fragments); 2) inappropriate behavior observed during the archeointensity experiments, either due to an alteration of the magnetic mineralogy or to the presence of a strong secondary magnetization component (∼43% of rejected fragments); and 3) uncertainties at the fragment level exceeding the threshold value of 5% of the corresponding mean (∼27% of rejected fragments). This led to the rejection of one group of fragments (YT12) for which no fragment was successfully analyzed. Group-mean intensity values could also not be determined for four groups because of an insufficient number of retained fragments (i.e. less than 3), YT02 and YT08 with only one fragment, and YT09 and YT18 with two fragments each (Table S2). The other groups contain from three to six fragments.

Fig. 6 exhibits the archeointensity data obtained at the specimen level for four different groups of fragments. They illustrate the limited scatter in the results obtained at the level of each group of fragments after the use of the 3σ rejection test for detecting outliers. This test allowed us to eliminate 13 fragments (Table S2). At this stage, only two groups of fragments were eliminated because the standard deviation of their mean intensities is larger than 5 μT (YT05 and YT13). Twenty-three groups of fragments of 30 originally were therefore successfully analyzed. The standard deviation of their means ranges from 0.6 μT to 5.0 μT (with an average of 1.8 ± 1.2 μT), or from 1.9% to 11.5% (with an average of 5.0 ± 3.1%) of the corresponding means.

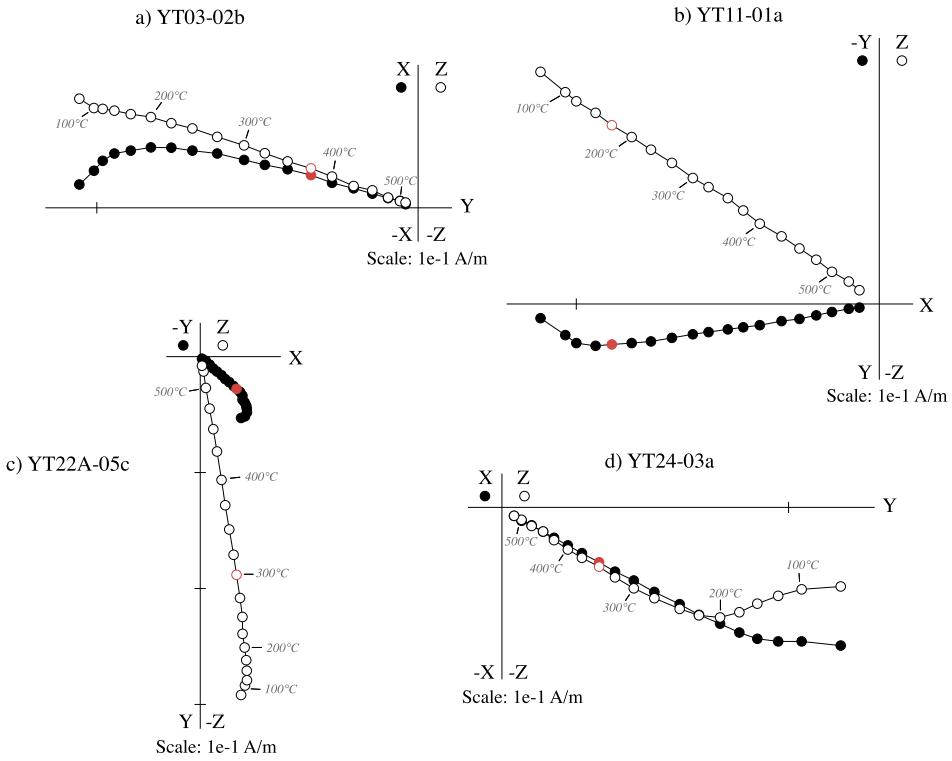

Fig. 5. Examples of thermal demagnetization diagrams obtained using the Triaxe protocol. The red point in each diagram indicates the directional data at T1′ (see text for explanation). Open (closed) symbols refer to the inclinations (declinations) in the orthogonal vector diagrams. (For interpretation of the references to color in this figure legend, the reader is referred to the web version of this article.)

The mean archeointensity values are displayed in Fig. 7 according to their stratigraphic position. They are reported both at the fragment level (including the data discarded) and at the level of the different groups of fragments after the use of the 3σ rejection test. From the 23 groups of fragments retained, we observe an overall step-like evolution, with a marked decrease in intensity by ∼12 μT around stratigraphic level ∼5 m (Table 1). The intensity values abruptly change from 43.8 ± 2.4 μT (the mean intensity value derived from seven groups in the lower part of the sequence, i.e. from groups YT23 to YT29) to 32.2 ± 1.4 μT (from 14 groups between YT21 and YT01). However, this change is accompanied by a "rebound" as group YT22 with a stratigraphic position between 4.60 and 4.70 m yields a mean intensity value of 44.3 ± 1.4 μT, whereas the underlying group YT22A (stratigraphic position 4.80–5.10 m) yields a mean intensity value of 31.0 ± 2.3 μT (Fig. 7).

The information conveyed by the results of the 3σ rejection test is also of interest. Detecting an outlier in several superimposed archeological layers as we did for 13 groups of fragments (Table 1) may arise from two different situations. For instance, outliers were detected in groups YT21, YT22 and YT22A that define the intensity peak previously mentioned around 4.6 m (Fig. 7). In this case, their presence may reflect the interdependence between the duration of the age interval associated with these archeological layers and the occurrence of large and rapid geomagnetic field intensity fluctuations during the same time interval. Hence, a fragment considered as an outlier may nevertheless belong to the same time interval than the other fragments of the same group. The same interpretation may stand for groups YT25 and YT26 that, we note, immediately underlie two groups of fragments (YT23 and YT24) possessing mean intensity values with relatively large standard deviations of 4.5 and 5.0 μT (∼11.5% of the corresponding means) but for which the 3σ rejection test was either unsuccessful or not possible. However, the detection of outliers appears widespread through the entire Yarim Tepe II sequence, in particular for groups YT01 and YT03 located at the top of the hill where stratigraphic disturbances did likely occur because of the emplacement of graves and pits. This seems to favor a second option in which an outlier comes from another archeological layer (or time interval) relative to that of the other fragments of the same group. This option, leading to the questioning of the homogeneity or integrity of the archeological layers assumed by the archeologists, is clearly less favorable for our archeomagnetic purposes. The important point to note here is the overall good consistency of the archeointensity results obtained in Yarim Tepe II after the use of the 3σ rejection test, with a weak intensity dispersion of less than 3.0 μT observed at the level of most groups of fragments. This suggests that the 3σ rejection test was efficient to eliminate most spurious data.

6. Construction of an age model for the Yarim Tepe II sequence

The pottery production found in Yarim Tepe II was unambiguously dated to the Halaf period, with some HUT levels (Munchaev and Merpert, 1981; Merpert and Munchaev, 1987, 1993; Bader, 1989; Amirov, 1994; Akkermans and Schwartz, 2003; Nieuwenhuyse et al., 2013). Further, based on results from excavations made in Syria over the past decades, several authors underlined the absence of Early Halaf pottery in Yarim Tepe II (e.g. Campbell, 2007; Robert, 2010; Bernbeck and Nieuwenhuyse, 2013). To better constrain this issue, we carried out AMS radiocarbon dating (Beta Analytic laboratory) of bone fragments, ∼20–30 g each, from three different stratigraphic levels in the lower half of the sequence: 3.80–4.30 m (reference Beta-453545, 6620 ± 30 BP: 5621–5492 cal. BC at 95%), 5.60–05.80 m (reference Beta-456967, 6810 ± 30 BP: 5736–5643 cal. BC at 95%) and 6.25–6.50 m (reference Beta-453547, 6730 ± 40 BP: ∼5718–5564 cal. BC at 95%). The livestock discovered in Yarim Tepe II principally consists of cattle, sheep and goats as attested by the finding of their teeth. The bone fragments that were analyzed therefore likely originate from these animals. The calendar ages obtained using the OxCal program with the INT-

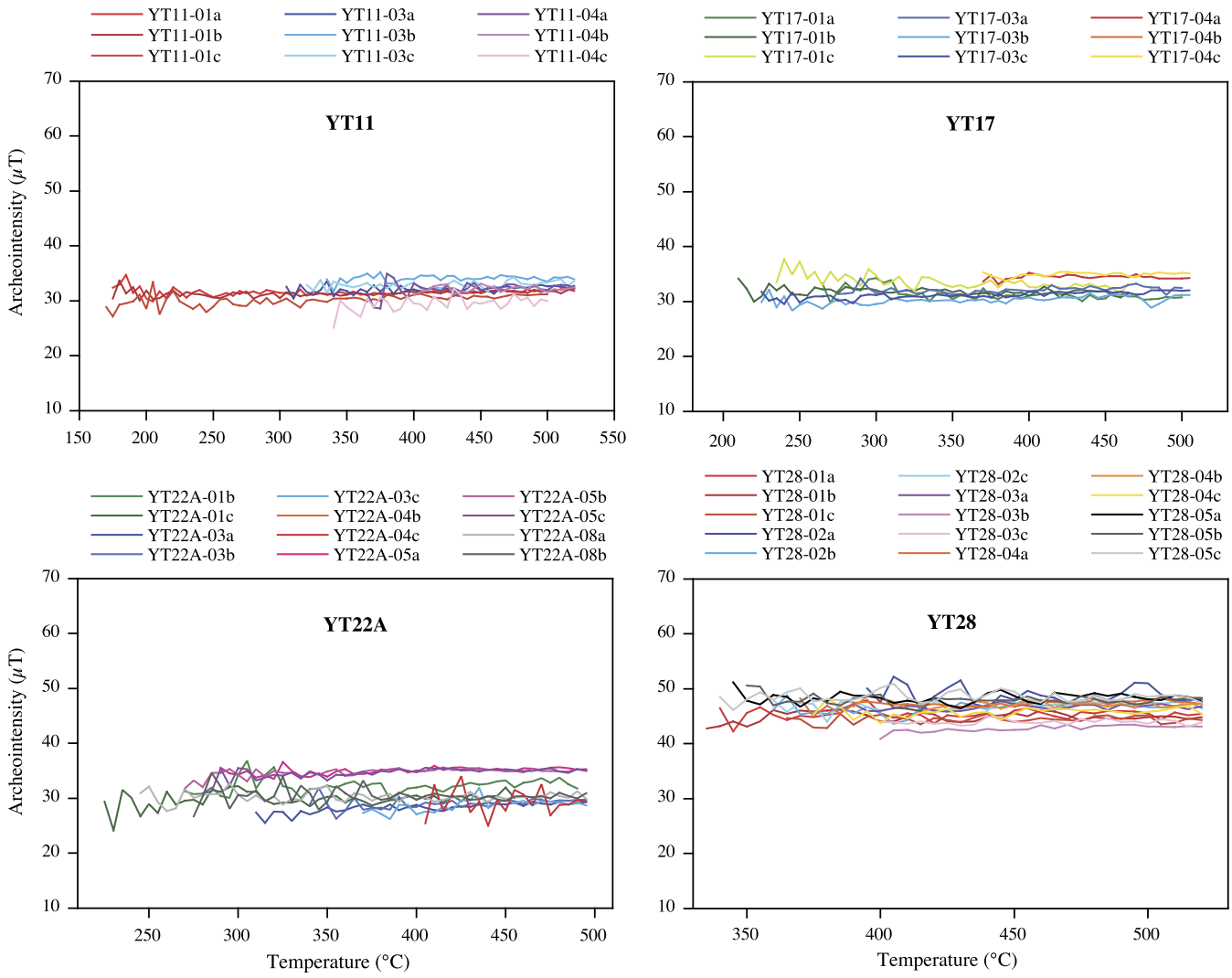

Fig. 6. R′(Ti) data obtained at the specimen level for four different groups of fragments after the use of the 3σ rejection test (see text). The data were first averaged at the level of each specimen (i.e. all data from each curve), these results were next averaged at the level of each fragment, and the latter mean values were finally averaged at the level of each group of fragments.

CAL13 calibration curve (Reimer et al., 2013) fall within the Middle Halaf and the Late Halaf, according to the chronology currently considered for the Halaf (Fig. 8). These new results thus strengthen the consideration on the age of Yarim Tepe II. Hereafter, we will consider the Middle Halaf time interval dated to between 5750 BC and 5550 BC, the Late Halaf between 5550 BC and 5300 BC and finally the Halaf-Ubaid Transitional period ranging from 5300 BC to 5000 BC (e.g. Campbell, 2007; Bernbeck and Nieuwenhuyse, 2013; Molist et al., 2013).

To report the new archeointensity data from Yarim Tepe II as a function of time, we constructed an age model using a bootstrap procedure that relies on the stratigraphic position of the different groups of fragments and on several tie-points available within the sequence. The latter are the three radiocarbon dates obtained in the present study and the three archeological boundaries traced by the archeologists. These are the Early Halaf-Middle Halaf boundary at the bottom of the sequence (~7.0 m), the Middle Halaf–Late Halaf boundary at ~4.80 m and the Late Halaf–HUT boundary at ~2.20 m. Uniform uncertainties of 20 cm (±10 cm) were attributed to the stratigraphic position of these boundaries, that is the typical thickness of the archeological layers defined by the archeologists (Table 1). Furthermore, we arbitrarily attributed reasonable uncertainties (1σ) of 25 yr to the age of the Early Halaf-Middle Halaf and Middle Halaf–Late Halaf boundaries currently considered in the Halafian chronology (5750 BC and 5550 BC, respectively; see references above), whereas the value was chosen higher (1σ = 37.5 yr) for the Late Halaf–HUT boundary (5300 BC) in order to take into account of the fact that its age is arguably less well known (Campbell, 2007; Campbell and Fletcher, 2010; and see below). The age of the groups of fragments archeologically dated to the HUT period was necessarily derived from another approach. Here we made the rough approximation of a constant accumulation rate for this part of the sequence, with a rate (0.94 cm/yr) derived from the other part of the Yarim Tepe II sequence using the same assumption but with a variability (1σ) of 25% around this value.

10,000 random samples were considered for the bootstrap using a uniform sampling for the depths and a Gaussian sampling for the ages of the three archeological boundaries. For the three radiocarbon dates, the random sampling was conducted according to each probability distribution resulting from their calibration using INTCAL13. The results of the age model are reported in Fig. 8 (see also Table 1). The ages obtained exhibit a rather smooth evolution, which does not significantly change if the free parameters of the computations are modified (i.e. the uncertainties on the exact stratigraphic position and age of the three archeological boundaries). Also interesting is the fact the ages that would be derived using the assumption of a constant accumulation rate through the

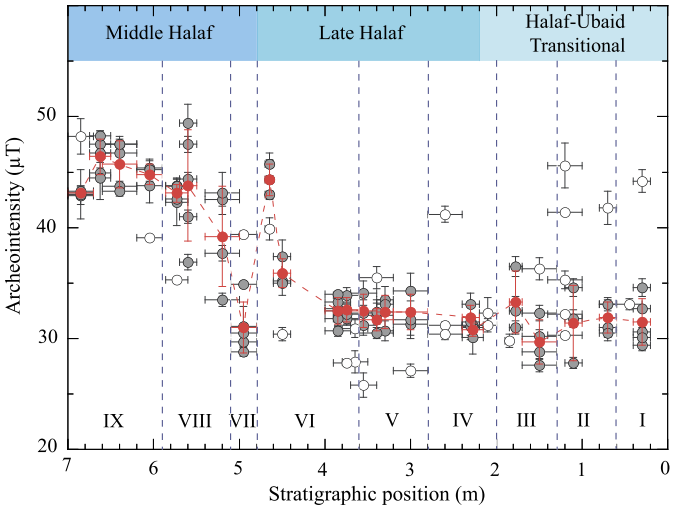

Fig. 7. New archeointensity results from Yarim Tepe II reported as a function of their stratigraphic position in the 7-m thick sequence of archeological deposits. The retained data are exhibited both at the fragment level (grey dots) and at the level of each group of fragments (red dots). White dots refer to intensity values at the fragment level that were not considered further either because they were eliminated by the 3σ rejection test, or the number of suitable fragments at the group level was less than 3 or because the standard deviation at the group level was larger than 5.0 μT. Archeological subdivisions according to Munchaev and Merpert (1981) and Amirov (1994) are also indicated on the figure. The archeological levels are labeled from I to IX. (For interpretation of the references to color in this figure legend, the reader is referred to the web version of this article.)

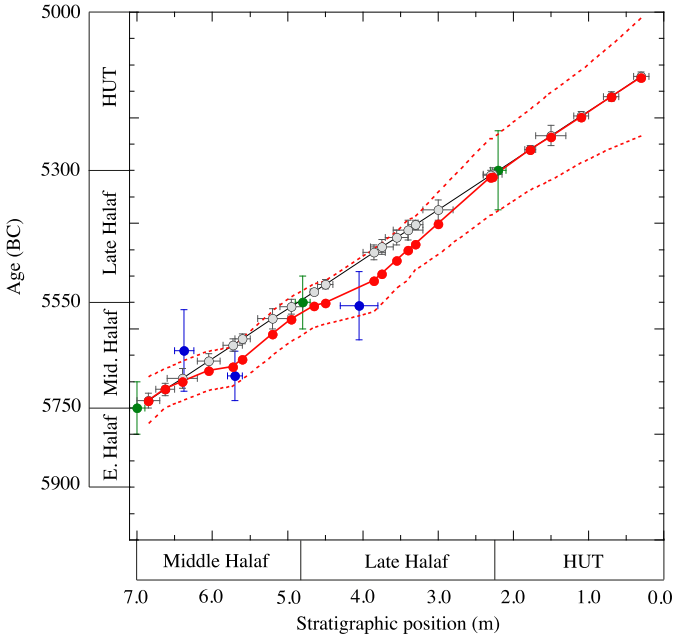

Fig. 8. Modeled ages derived for the 23 groups of fragments successfully analyzed in Yarim Tepe II (red dots). See the text for a description of the age model, which relies on a bootstrap approach with six different tie-points (in blue, the AMS radiocarbon dates obtained from three bone fragments; in green, the three archeological boundaries traced by the archeologists inside the Yarim Tepe II sequence). The red dotted lines show the age envelope of the groups of fragments at 95%. The age uncertainties of the tie-points are also reported at 95%. The grey dots exhibit the age of the groups of fragments derived from the rough assumption of a constant accumulation rate through the entire Yarim Tepe II sequence (see text). In this case, note that the ages are uniformly distributed inside the age intervals reported. (For interpretation of the references to color in this figure legend, the reader is referred to the web version of this article.)

entire Yarim Tepe II sequence (grey dots) lie inside the 95% envelope given by the bootstrap procedure (red dotted lines). This means that, considering the available constraints, any option for the computation of an age model in Yarim Tepe II gives relatively similar results.

7. Discussion

7.1. Intensity secular variation in the Near East and Eastern Europe during the 6th millennium BC

There now exists two principal regional archeointensity data sets for the 6th millennium BC, one obtained in Northern Mesopotamia (Syria and Iraq; Gallet et al., 2015 and this study), the second in Eastern Europe (Bulgaria; see Kovacheva et al., 2014 for a synthesis).

The series of new archeointensity data from Yarim Tepe II comes as a complement to previous Halafian and HUT results obtained in Northern Mesopotamia from the archeological sites of Tell Halula and Tell Masaikh (Gallet et al., 2015). A comparison between these data sets is shown in Fig. 9a after conversion of the intensity values into Virtual Axial Dipole Moments (VADM). This comparison first appears quite problematic. However, similarities exist with, in both cases, the occurrence of a peak in intensity during the Late Halaf and low intensity values during the HUT time interval. It is possible to reconcile the two records owing to the facts that the Late Halaf data from Tell Halula possess a stratigraphic relationship, with five superimposed occupation levels, and that the latter were dated making the rough approximation of an equi-temporal distribution for these occupation levels within the entire Late Halaf period (see discussion in Gallet et al., 2015). As a result, there is no inherent impossibility that these occupation levels (nine groups of fragments) actually date from the older part of the Late Halaf. The site of Tell Halula would then have been abandoned during the recent part of the Late Halaf. To illustrate this possibility, the Late Halaf intensity results from Tell Halula were also reported in Fig. 9a assuming that the site was only occupied during the first one-third of this time interval (light blue dots and grey arrows). From this rough approximation, again perfectly compatible with the archeological constraints, a satisfactory correlation emerges between the Syrian and Iraqi data, with in both cases, a short lasting intensity peak around 5500 BC at the beginning of the Late Halaf period.

Situated relatively close to the Northern Mesopotamian area, it is most probable that the Bulgarian archeointensity results (Kovacheva et al., 2014) have recorded the same geomagnetic field intensity variations. The age of 16 of 41 available data was constrained using radiocarbon dating, in complement with archeological and stratigraphic arguments. The VADM values are reported in Fig. 9b with a distinction between the results the reliability of which was constrained or not by the use of partial-TRM (pTRM) checks during the experimental procedure (black and grey dots, respectively). There is no evidence for a bias between the two series of data, as both series exhibit a similar decreasing trend between ~5800 BC and ~5600 BC and an increasing trend between ~5400 BC and ~5000 BC. In contrast, no intensity result with pTRM checks allows one to strengthen the occurrence of the intensity peak at ~5500 BC (Fig. 9b). Therefore, only the good agreement observed during the other periods suggests that a major bias in the data around 5500 BC is rather unlikely.

Fig. 9b also shows the average curve computed from the Bulgarian archeointensity data using the Monte Carlo Markov Chain approach developed by Lanos (2004) (and with further improvements more recently achieved by P. Lanos). These results reveal the existence of two distinct short-lasting intensity peaks during the 6th millennium BC: a first peak around 5800 BC, which would have occurred during the Early Halaf according to the Halafian chronology, and a second peak around 5500 BC. The latter is clearly

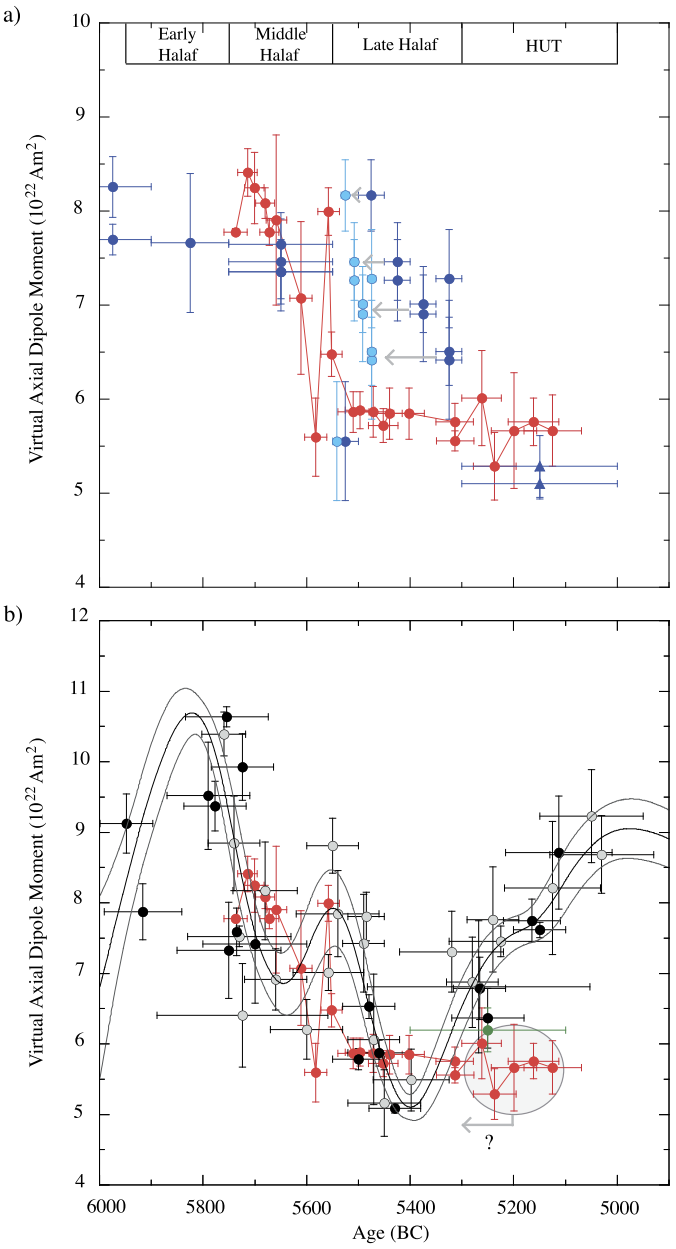

Fig. 9. Comparison between the archeointensity data available in Northern Mesopotamia (Syria, Iraq) and in Eastern Europe (Bulgaria, Greece) for the 6th millennium BC. a) Northern Mesopotamian data set. Comparison of the new data from Yarim Tepe II (red dots) with the archeointensity results previously obtained by Gallet et al. (2015) in Tell Halula and Tell Masaikh (dark-blue dots and triangles, respectively). The light-blue dots show the Late Halaf data obtained from Tell Halula assuming that this site was only occupied during the first one-third of this time interval (see text for explanations). b) Yarim Tepe II (red dots) and Eastern European data sets. The black (resp. grey) dots show the Bulgarian archeointensity data (Kovacheva et al., 2014), the reliability of which was constrained (resp. not) by the use of pTRM checks during the experimental procedure. The green dot exhibits the single result obtained in Greece by Fanjat et al. (2013). (For interpretation of the references to color in this figure legend, the reader is referred to the web version of this article.)

reminiscent of the one observed in the Middle East from the Tell Halula and Yarim Tepe II data (Fig. 9a). The average Bulgarian curve suggests a duration of ~100–200 yr for this peak, whereas the data from Yarim Tepe II may indicate a shorter duration of only a few decades. At least a part of this difference may arise from the smoothing resulting from the construction of the Bulgarian curve, but it is also important to note the uncertainties existing on the accuracy and reliability of the dating of the different (Bulgarian, Iraqi and Syrian) data sets.

The comparison between the results dated to the end of the 6th millennium BC is more problematic. The HUT data from Tell Masaikh and Yarim Tepe II are all very similar, with low VADM of ~5–6·10^{22} Am^2 (~30–33 μT, Figs. 7, 9a), whereas the data from Bulgaria show a significant increasing trend with VADM reaching ~9·10^{22} Am^2 at the end of the 6th millennium (Fig. 9b). A large part of this discrepancy would be resolved if the Syrian and Iraqi results were dated from the very beginning of the HUT period, which is not in contradiction with the available archeological constraints. Furthermore, a quite excellent agreement would be obtained if the Late Halaf–HUT boundary were to be shifted by about one century relative to the Halafian chronology presently considered (e.g. Molist et al., 2013). Such a possibility seems reasonable thanks to recent, yet unpublished data from Tell Begum in Iraqi Kurdistan (O. Nieuwenhuyse, personal communication; see also discussion in Campbell, 2007 and Campbell and Fletcher, 2010), but it still requires further work.

From the archeointensity data obtained in Yarim Tepe II, it is possible to determine the intensity variation rates associated with the peak at ~5500 BC using a bootstrap procedure with a Gaussian sampling for both the intensities and the ages. We therefore performed the computations between groups YT22A and YT22 and between YT22 and YT21 that define the ascending and descending branches of the peak, respectively. Because there are an overlap of the age intervals and a time-order relationship between the different groups of fragments, the intensity variation rates obtained from the bootstrap are not normally distributed and only the determination of the maximum of probability is meaningful. The latter amounts to 0.23 μT/yr in the first case and 0.19 μT/yr in the second case (Fig. S2). Likewise, the most probable intensity variation rate associated with the rapid decrease in intensity between groups YT24 and YT22A before the occurrence of the intensity peak reaches ~0.14 μT/yr. This order of magnitude, between ~0.15 and ~0.25 μT/yr, is slightly higher than the maximum intensity variation rate prevailing in the recent field (Livermore et al., 2014). It appears similar to that of the variation rates observed in Western Europe around 700 BC (Hervé et al., 2017) and probably during the 10th century AD (Genevey et al., 2013, 2016). The rate of all these variations appears significantly lower than that of the intensity variations associated with the geomagnetic spikes (e.g. Ben-Yosef et al., 2009; Shaar et al., 2011, 2016), while it would characterize that of the intensity peaks that were associated with archeomagnetic jerks (Gallet et al., 2003, 2014).

7.2. Regional vs global geomagnetic field intensity variations during the 6th millennium BC

For testing the global vs regional nature of the geomagnetic field intensity variations observed in the Near East and in Eastern Europe, it is necessary to compare the latter data with those available in other distant regions, whether obtained from archeological artifacts or volcanic rocks. However, examining databases such as ArcheoInt or Geomagia50.v3 (Genevey et al., 2008; Brown et al., 2015) shows that they are rare and often do not meet modern reliability criteria. If minimalist selection criteria are considered, such as the need for pTRM checks, at least two samples analyzed per intensity value and age uncertainties of less than ±200 yr established from a convincing approach, there is currently almost no data allowing one to further document the geomagnetic field intensity evolution during the 6th millennium BC. In particular, several data from Central Asia, Caucasus and Western Europe (Spain) were eliminated because of their large or poorly constrained age uncertainties. More than a dozen intensity data obtained from long cores SOH1 and SOH4 drilled in

the Hawaiian Kilauea volcano had to be eliminated because they were published without age uncertainties (e.g. Laj et al., 2002; Gratton et al., 2005). For both cores, their dating was established from a rough age model relying on a too limited number of radiometric tie-points, leading to a questionable reliability (Tema et al., 2017). For this reason, Tema et al. (2017) also discarded these results from their recent compilation of the Hawaiian intensity data available for the Holocene.

Hence, as a consequence of the lack of data, it is not yet possible to specify to what extent the intensity fluctuations observed in the Near East and Eastern Europe during the 6th millennium BC are global or only regional features, and can be assigned to dipole or non-dipole field variations. However, the shortness of the intensity peaks observed around 5800 BC and 5500 BC suggests that they are more likely to be principally related to non-dipole field components. As was suggested by Gallet et al. (2009) to explain archeomagnetic jerks in Western Europe, these peaks might be related to episodes of maximum geomagnetic field hemispheric asymmetry involving the behavior of the dipole and quadrupole field components. It is worth pointing out that the Hawaiian area, which is approximately 180° away in longitude from the Near East and Eastern Europe, would be a very promising region to test a such geomagnetic origin.

On another hand, it is worth stressing that the scarcity of the data available for the 6th millennium BC prevents the computation of reliable and accurate global field models over this time interval. As was previously noted by Gallet et al. (2015), the models that were nevertheless computed for this period (e.g. Pavón-Carrasco et al., 2014; Nilsson et al., 2014) are further penalized by the fact that they incorporated a large number of data from the Near East (Tell Sotto, Iraq; Nachasova and Burakov, 1998) supposedly dated from the 6th millennium BC, whilst that are actually unambiguously dated from the 7th millennium BC (see for instance Bernbeck and Nieuwenhuyse, 2013). It thus follows that the comparison of the archeointensity data obtained in the Near East and Bulgaria with the intensity values expected from the global geomagnetic field models does not provide further information to deciphering the geomagnetic origin of the intensity peaks discussed here.

8. Concluding remarks

In spite of its antiquity, the Halaf period appears as a privileged time interval to bring interesting new constraints on rapid geomagnetic field evolution over decadal and centennial timescales. The archeomagnetic study led in Yarim Tepe II clearly shows the occurrence in the Near East of a short-lasting geomagnetic field intensity peak, perhaps over only a few decades, around 5500 BC (during the early Late Halaf), in agreement with previous Bulgarian and Syrian data. In addition, the Bulgarian data argue for the occurrence of another intensity peak around 5800 BC, during the Early Halaf. The intensity secular variation in the Near East and Eastern Europe during the 6th millennium BC was thus principally punctuated by two distinct decadal- to centennial-scale peaks.

The intensity variation rates associated with the rapid intensity fluctuations observed in Yarim Tepe II reach a value as high as ∼0.15–0.25 μT/yr. Being slightly stronger than the maximum rates prevailing in the modern field, this value appears quite similar to that of other rapid intensity variations that were evidenced in Western Europe during more recent archeological periods. Unfortunately, the scarcity of the intensity results dated to the 6th millennium BC still obtained worldwide prevents us from deciphering to what extent the geomagnetic field intensity variations observed in the Near East and in Eastern Europe do represent rapid fluctuations in the dipole and/or non-dipole field components.

From an archeological point of view, the discrepancy observed for the end of the 6th millennium BC between the Northern Mesopotamian (Syria, Iraq) and Bulgarian archeointensity data sets could help in deciphering the age and duration of the Halal-Ubaid Transition period, that are yet poorly understood. Archeointensity investigations focused on the 6th millennium BC should therefore be continued.

Acknowledgements

This study was financed by grant N 14.Z50.31.0017 of the Russian Ministry of Science and Education. We thank Anna Gómez Bach, Miquel Molist, Olivier Nieuwenhuyse, Béatrice Robert, Pascal Butterlin, Phil Livermore and Alexandre Fournier for interesting discussions. Special thanks to Fernand Lopes for his help in computing the age model. We are also very grateful to Maxime Le Goff and Agnès Genevey for their continued and unselfish assistance and stimulating discussions. We thank F.J. Pavón-Carrasco and two anonymous reviewers for helpful comments. This is IPGP contribution no. 3894.

Appendix A. Supplementary material

Supplementary material related to this article can be found online at https://doi.org/10.1016/j.epsl.2017.11.013.

References

Akkermans, P.M.M.G., Schwartz, G.M., 2003. The archaeology of Syria. From complex hunter-gatherers to early urban societies (ca. 16,000–300 BC). In: Cambridge World Archaeology. Cambridge University Press, New York, p. 467.

Amirov, S., 1994. The Morphology of Halafian Culture Ceramics Based on the Material Collected from the Settlement Yarim Tepe II (in Russian). Doctoral thesis, Moscow. 144 pp.

Bader, N., 1989. Earliest Cultivators in Northern Mesopotamia. The Investigations of Soviet Archaeological Expedition in Iraq at Settlements Tell Magzaliya, Tell Sotto, and Kül Tepe. Nauka, Moscow.

Ben-Yosef, E., Tauxe, L., Levy, T.E., Shaar, R., Ron, H., Najjar, M., 2009. Geomagnetic intensity spike recorded in high resolution slag deposit in southern Jordan. Earth Planet. Sci. Lett. 287, 529–539.

Bernbeck, J., Nieuwenhuyse, O.P., 2013. Established paradigms, current disputes and emerging themes: the state of research on the Late Neolithic in Upper Mesopotamia. In: Interpreting the Late Neolithic of Upper Mesopotamia. In: Publications on Archaeology of the Leiden Museum of Archaeology (PALMA). Brepols pub., Turnhout, Belgium, pp. 17–37.

Brown, M.C., Donadini, F., Korte, M., Nilsson, A., Korhonen, K., Lodge, A., Lengyel, S.N., Constable, C.G., 2015. GEOMAGIA50.v3: 1. General structure and modifications to the archeological and volcanic database. Earth Planets Space 67, 83.

Campbell, S., 2007. Rethinking Halaf chronology. Paleorient 33, 103–136.

Campbell, S., Fletcher, A., 2010. Questioning the Halaf-Ubaid transition. In: Carter, R.A., Philip, G. (Eds.), Beyond the Ubaid: Transformation and Integration in the Late Prehistoric Societies of the Middle East. In: SAOC: Studies in Ancient Oriental Civilization, vol. 63. The Oriental Institute of the University of Chicago, pp. 69–83.

Dumberry, M., Finlay, C., 2007. Eastward and westward drift of the Earth's magnetic field for the last three millennia. Earth Planet. Sci. Lett. 254, 146–157.

Dunlop, D.J., 2002. Theory and application of the day plot (Mrs/Ms versus Hcr/Hc) 1. Theoretical curves and tests using titanomagnetite data. J. Geophys. Res. 107. 2056.

Ertepinar, P., Langereis, C.G., Biggin, A.J., Frangipane, M., Matney, T., Ökse, T., Engin, A., 2012. Archaeomagnetic study of five mounds from upper Mesopotamia between 2500 and 700 BC: further evidence for an extremely strong geomagnetic field ca. 3000 years ago. Earth Planet. Sci. Lett. 357–358, 84–98.

Fanjat, G., Aidona, E., Kondopoulou, D., Camps, P., Rathossic, C., Poidras, T., 2013. Archeointensities in Greece during the Neolithic period: new insights into material selection and secular variation curve. Phys. Earth Planet. Inter. 215, 29–42.

Fournier, A., Gallet, Y., Usoskin, I., Livermore, P.W., Kovaltsov, G.A., 2015. The impact of geomagnetic spikes on the production rates of cosmogenic ^{14}C and ^{10}Be in the Earth's atmosphere. Geophys. Res. Lett. 42, 2759–2766.

Gallet, Y., Genevey, A., Courtillot, V., 2003. On the possible occurrence of 'archaeomagnetic jerks' in the geomagnetic field over the past three millennia. Earth Planet. Sci. Lett. 214, 237–242.

Gallet, Y., Le Goff, M., 2006. High-temperature archeointensity measurements from Mesopotamia. Earth Planet. Sci. Lett. 241, 159–173.

Gallet, Y., Genevey, A., Le Goff, M., Fluteau, F., Eshraghi, S.A., 2006. Possible impact of the Earth's magnetic field on the history of ancient civilizations. Earth Planet. Sci. Lett. 246, 17–26.

Gallet, Y., Hulot, G., Chulliat, A., Genevey, A., 2009. Geomagnetic field hemispheric asymmetry and archeomagnetic jerks. Earth Planet. Sci. Lett. 284, 179–186.
Gallet, Y., D'Andrea, M., Genevey, A., Pinnock, F., Le Goff, M., Matthiae, P., 2014. Archaeomagnetism at Ebla (Tell Mardikh, Syria). New data on geomagnetic field intensity variations in the Near East during the Bronze Age. J. Archaeol. Sci. 42, 295–304.
Gallet, Y., Molist, M., Genevey, A., Clop Garcia, X., Thébault, E., Gómez Bach, A., Le Goff, M., Robert, B., Nachasova, I., 2015. New Late Neolithic (c. 7000–5000 BC) archeointensity data from Syria. Reconstructing 9000 years of archeomagnetic field intensity variations in the Middle East. Phys. Earth Planet. Inter. 238, 89–103.
Genevey, A., Gallet, Y., Margueron, J., 2003. Eight thousand years of geomagnetic field intensity variations in the eastern Mediterranean. J. Geophys. Res. 108, 2228.
Genevey, A., Gallet, Y., Constable, C., Korte, M., Hulot, G., 2008. ArcheoInt: an upgraded compilation of geomagnetic field intensity data for the past ten millennia and its application to the recovery of the past dipole moment. Geochem. Geophys. Geosyst. 9 (4), Q04038.
Genevey, A., Gallet, Y., Rosen, J., Le Goff, M., 2009. Evidence for rapid geomagnetic field intensity variations in Western Europe over the past 800 years from new archeointensity French data. Earth Planet. Sci. Lett. 284, 132–143.
Genevey, A., Gallet, Y., Thébault, E., Jesset, S., Le Goff, M., 2013. Geomagnetic field intensity variations in Western Europe over the past 1100 years. Geochem. Geophys. Geosyst. 14 (8), 2858–2872.
Genevey, A., Gallet, Y., Jesset, S., Thébault, E., Bouillon, J., Lefèvre, A., Le Goff, M., 2016. New archeointensity data from French Early Medieval pottery production (6th–10th century AD). Tracing 1500 years of geomagnetic field intensity variations in Western Europe. Earth Planet. Sci. Lett. 257, 205–219.
Gratton, M.N., Shaw, J., Herrero-Bervera, E., 2005. An absolute palaeointensity record from SOH1 lava core, Hawaii using the microwave technique. Phys. Earth Planet. Inter. 148, 193–214.
Hartmann, G., Genevey, A., Gallet, Y., Trindade, R., Etchevarne, C., Le Goff, M., Afonso, M., 2010. Archeointensity in Northeast Brazil over the past five centuries. Earth Planet. Sci. Lett. 296, 340–352.
Hartmann, G., Genevey, A., Gallet, Y., Trindade, R., Le Goff, M., Najjar, R., Etchevarne, C., Afonso, M., 2011. New historical archeointensity data from Brazil: evidence for a large regional non-dipole field contribution over the past few centuries. Earth Planet. Sci. Lett. 306, 66–76.
Hervé, G., Fassbinder, J., Gilder, S., Metzner-Nebelsick, C., Gallet, Y., Genevey, A., Schnepp, E., Geisweid, L., Pütz, A., Reub, S., Wittenborn, F., Flontas, A., Linke, R., Riedel, G., Walter, F., Westhausen, I., 2017. Fast geomagnetic field intensity variations between 1400 and 400 BCE: new archaeointensity data from Germany. Phys. Earth Planet. Inter. 270, 143–156.
Hirose, K., Labrosse, S., Hernlund, J., 2013. Composition and state of the core. Annu. Rev. Earth Planet. Sci. 41, 657–691.
Kostadinova-Avramova, M., Kovacheva, M., Boyadzhiev, Y., 2014. Contribution of stratigraphic constraints of Bulgarian prehistoric multilevel tells and a comparison with archaeomagnetic observations. J. Archaeol. Sci. 43, 227–238.
Kovacheva, M., Kostadinova-Avramova, M., Jordanova, N., Lanos, P., Boyadziev, Y., 2014. Extended and revised archaeomagnetic database and secular variation curves from Bulgaria for the last eight millennia. Phys. Earth Planet. Inter. 236, 79–94.
Laj, C., Kissel, C., Scao, V., Beer, J., Thomas, D.M., Guillou, H., Muscheler, R., Wagner, G., 2002. Geomagnetic intensity and inclination variations at Hawaii for the past 98 Kyr from core SOH-4 (Big Island): a new study and a comparison with existing contemporary data. Phys. Earth Planet. Inter. 129, 205–243.
Lanos, P., 2004. Bayesian inference of calibration curves: application to archaeomagnetism. In: Buck, C.E., Millard, A.R. (Eds.), Tools for Constructing Chronologies: Crossing Disciplinary Boundaries. Springer, London, pp. 43–82.
Le Goff, M., Gallet, Y., 2004. A new three-axis vibrating sample magnetometer for continuous high-temperature magnetization measurements: applications to paleo- and archeo-intensity determinations. Earth Planet. Sci. Lett. 229, 31–43.
Livermore, P.W., Fournier, A., Gallet, Y., 2014. Core-flow constraints on extreme archeomagnetic intensity changes. Earth Planet. Sci. Lett. 387, 145–156.
Molist, M., Anfruns, J., Bofill, M., Borrell, F., Buxy, R., Clop, X., Cruells, W., Faura, J.M., Ferrer, A., Gómez, A., Guerrero, E., Saca, M., Tornero, C., Vicente, O., 2013. Tell Halula (Euphrates Valley, Syria): new approach to VII and VI millennia cal. B.C. in Northern Levant framework. In: Interpreting the Late Neolithic of Upper Mesopotamia. In: Publications on Archaeology of the Leiden Museum of Archaeology (PALMA). Brepols pub., Turnhout, Belgium, pp. 443–455.
Merpert, N.J., Munchaev, R.M., 1987. The earliest levels at Yarim Tepe I and Yarim Tepe II in Northern Iraq. Iraq 49, 1–36.
Merpert, N.J., Munchaev, R.M., 1993. Yarim Tepe II: the Halaf levels. In: Yoffee, N., Clark, J. (Eds.), Early Stages in the Evolution of Mesopotamian Civilizations: Soviet Excavatins in Northern Iraq. University of Arizona Press, Tucson, pp. 129–162.
Munchaev, R.M., Merpert, N.J., 1981. Earliest Agricultural Settlements of Northern Mesopotamia. The Investigation of Soviet Expedition in Iraq. Nauka, Moscow (in Russian).
Nachasova, I., Burakov, K., 1995. Archaeointensity of the geomagnetic field in the fifth millennium B.C. in northern Mesopotamia. Geomagn. Aeron. 35, 398–402.
Nachasova, I., Burakov, K., 1998. Geomagnetic variations in the VI–V millennia B.C. Geomagn. Aeron. 38, 502–505.
Nieuwenhuyse, O.P., Bernbeck, R., Akkermans, P.M.M.G., Rogasch, J., 2013. Interpreting the late neolithic of upper Mesopotamia. Publications on Archaeology of the Leiden Museum of Archaeology (PALMA). Brepols pub., Turnhout, Belgium, p. 520.
Nilsson, A., Holme, R., Korte, M., Suttie, N., Hill, M., 2014. Reconstructing Holocene geomagnetic field variation: new methods, models and implications. Geophys. J. Int. 198, 229–248.
Pavón-Carrasco, F.J., Osete, M.L., Torta, J.M., De Santis, A., 2014. A geomagnetic field model for the Holocene based on archaeomagnetic and lava flow data. Earth Planet. Sci. Lett. 388, 98–109.
Reimer, P.J., Bard, E., Bayliss, A., Warren, J.B., Blackwell, P., Ramsey, C.B., Buck, K., Cheng, H., Edwards, L., Friedrich, M., Grootes, P.M., Guilderson, T.P., Haflidason, H., Hajdas, I., Hatté, C., Heaton, T.J., Hoffmann, D.L., Hogg, A.G., Hughen, K.A., Kaiser, K.F., Kromer, B., Manning, S.W., Niu, M., Reimer, R.W., Richards, D.A., Scott, E.M., Southon, J.R., Staff, R.A., Turney, C.S., Van der Plicht, J., 2013. IntCal13 and Marine13 radiocarbon age calibration curves 0–50,000 years cal BP. Radiocarbon 55 (4), 1869–1887.
Robert, B., 2010. Développement et disparition de la production céramique halafienne: implications techniques et sociales à partir d'études de cas. PhD thesis. Université Lumière Lyon 2. 899 pp.
Shaar, R., Ben-Yosef, E., Ron, H., Tauxe, L., Agnon, A., Kessel, R., 2011. Geomagnetic field intensity: how high can it get? How fast can it change? Constraints from iron-age copper-slag. Earth Planet. Sci. Lett. 301, 297–306.
Shaar, R., Tauxe, L., Ron, H., Ebert, Y., Zuckerman, S., Finkelstein, I., Agnon, A., 2016. Large geomagnetic field anomalies revealed in Bronze to Iron Age archeomagnetic data from Tel Megiddo and Tel Hazor, Israel. Earth Planet. Sci. Lett. 442, 173–185.
Tema, E., Herrero-Bervera, E., Lanos, P., 2017. Geomagnetic field secular variation in Pacific Ocean: a Bayesian reference curve based on Holocene Hawaiian lava flows. Earth Planet. Sci. Lett. 478, 58–65.
Thellier, E., Thellier, O., 1959. Sur l'intensité du champ magnétique tesrrestre dans le passé historique et géologique. Ann. Geophys. 15, 285–376.